Abdominal Imaging

Staging accuracy of MR for pancreatic neuroendocrine tumor and imaging findings according to the tumor grade

Jung Hoon Kim,[1] Hyo Won Eun,[2] Young Jae Kim,[3] Joon Koo Han,[1] Byung Ihn Choi[1]

[1]Department of Radiology and Institute of Radiation Medicine, Seoul National University College of Medicine, 101 Daehang-no, Chongno-gu, Seoul 110-744, Republic of Korea

[2]Department of Radiology, Severance Hospital, Yonsei University College of Medicine, Seodaemun-ku, Shinchon-dong 134, Seoul 120-752, Republic of Korea

[3]Department of Radiology, Soonchunhyang University Hospital, 657 Hannam-Dong, Youngsan-Ku, Seoul 140-743, Republic of Korea

Abstract

Purpose: To investigate staging accuracy of MR for pancreatic neuroendocrine neoplasms (PNETs) and imaging findings according to the tumor grade.
Materials and methods: Our study consisted of 39 patients with PNET G1 ($n = 24$), PNET G2 ($n = 12$), and pancreatic neuroendocrine carcinoma (PNEC) ($n = 3$). All underwent preoperative MRI. Two radiologists retrospectively reviewed MR findings including tumor margin, SI on T2WI, enhancement patterns, degenerative change, duct dilation, and ADC value. They also assessed T-stage, N-stage, and tumor size. Statistical analyses were performed using Chi square tests, ROC analysis, and Fisher's exact test.
Results: Specific findings for PNEC or PNET G2 were ill-defined borders ($P = 0.001$) and hypo-SI on venous- and delayed-phase ($P = 0.016$). ADC value showed significant difference between PNET G1 and G2 ($P = 0.007$). The Az of ADC value for differentiating PNET G1 from G2 was 0.743. Sensitivity and specificity were 70% and 86%. Accuracy for T-staging was 77% ($n = 30$) and 85% ($n = 33$), and for N-staging was 92% ($n = 36$) and 87% ($n = 34$) with moderate agreement. T-stage showed significant difference according to tumor grade ($P < 0.001$), although there was no significant difference in tumor size or N-stage.
Conclusion: Ill-defined borders and hypo-SI on venous- and delayed-phase imaging are common findings of higher grade PNET, and ADC value is helpful for differentiating PNET G1 from G2. MR is useful for preoperative evaluation of T-, N-stage. Tumor size of PNET and T-stage showed significant difference according to tumor grade.

Key words: Magnetic resonance imaging—Diffusion-weighted magnetic resonance—Imaging—Pancreatic neuroendocrine tumor—WHO tumor classification—TNM stage

Pancreatic neuroendocrine neoplasms (PNETs) have traditionally been considered as a rare disease. In recent years, however, the diagnosed incidence of PNET has increased due to improved detection and classification methods. PNETs constitute a heterogeneous group of tumors that originate from neuroendocrine cells and they have great behavioral differences [1].

In 2010, the WHO published a classification of neuroendocrine tumor (NET) [2]. They classified NET into NET grade 1, NET grade 2, and neuroendocrine carcinoma (NEC). The proposed grading was based on the number of the mitotic count and the percentage of the Ki67 index. Although the new WHO classification is an important step toward defining the diverse tumor biology of NETs, it does not represent the tumor extent. For this reason the TNM staging also uses in PNET [3–6]. The classic grading system is based on histological differentiation, and the TNM staging system is based on the tumor extent. Therefore, accurate assessment of the tumor stage and grade is an essential step in the treatment planning for PNET.

Correspondence to: Jung Hoon Kim; email: Jhkim2008@gmail.com

Due to the recent MR technological developments, MR has developed into a useful imaging modality for the pancreas. Several previous studies have shown promising results using MRI, including MRCP for the detection, characterization, and staging of pancreatic tumors [7–11]. Furthermore, recently developed diffusion-weighted imaging (DWI) has led to improve detection and characterization of focal pancreatic lesions [12, 13]. Although there are several reports regarding the MR findings for PNETs, to our knowledge there are no previously reported studies regarding the diagnostic performance of MRI and DWI according to the WHO classification compared with the TN-stage of PNETs. Therefore, this study was designed to assess the staging accuracy of gadolinium-enhanced MRI and DWI for PNET and imaging findings according to the tumor grade.

Methods and materials

Patients

This study was approved by our institutional review board, and informed consent was not required. After conducting a computerized search of our hospital's pathology files and medical records from February 2006 to June 2011, we identified 61 patients with pathologically proven NET of the pancreas. Our inclusion criteria were (a) patients with pancreas NET who had undergone surgery at our hospital, (b) patients who underwent preoperative, contrast-enhanced MRI including MRCP before surgery, (c) a diagnosis of pancreatic NET based on the pathology examination of a surgical specimen, and (d) a tumor size larger than 0.5 cm. Thirty-nine patients were finally included in our retrospective study. There were 20 men and 19 women with a mean age of 53.9 years (age range, 37–72 years). The mean interval between the MR examination and the surgery was 15.3 days (range, 2–36 days). All patients had previously undergone surgery including pylorus-preserving pancreaticoduodenectomy (n = 17), Whipple surgery (n = 4), enucleation (n = 4), and distal pancreatectomy (n = 14). We retrospectively reviewed the gross and microscopic descriptions of the resected specimens described in the pathology reports. The demographic and clinical data are shown in Table 1.

MRI

All MRI examinations was performed on either a 1.5 T or on a 3 T superconducting system (Signa Excite HDX, GE Medical Systems, Milwaukee, WI, USA, n = 27; Verio, Siemens Medical Solutions, Erlangen, Germany, n = 12) using either an 8-channel (Signa Excite HDX) or a 32-channel (Verio), phased-array torso coil. Patients fasted for 8 h prior to the MR examination. The MR parameters of each sequence are summarized in Table 2. Our MR protocol for the pancreas included transverse,

Table 1. Demography and clinical data of patients with PNET

	No. (n = 39)
Mean age (years)	53.9 ± 9.5[a]
Male:female patient ratio	20:19
Tumor location	
Head	19 (49%)
Uncinate	2 (5%)
Body	10 (26%)
Tail	8 (21%)
Surgical procedure	
Whipple	4 (10%)
PPPD	17 (44%)
Enucleation	4 (10%)
Distal pancreatectomy	14 (36%)
Tumor function	
Functional	5
Non-functional	34

PPPD pylorus-preserving pancreaticoduodenectomy
[a] Mean tumor size ± standard deviation

T2-weighted images (T2WI), including a single-shot, fast spin-echo (SSFSE) or a half-Fourier acquisition, single-shot, turbo spin-echo (HASTE) sequence, transverse T1-weighted imaging (T1WI) including in-phase and opposed-phase spoiled gradient echo (GRE) techniques, breath-hold and respiratory-triggered MRCP images, and gadolinium-enhanced dynamic MRI using a fat-saturated, 3D-GRE sequence. Three MRCP methods were used for evaluation of the biliary and pancreatic duct anatomy: (1) the breath-hold, single-slice, rapid acquisition using the relaxation enhancement (RARE) technique, fast spin-echo (FSE) or turbo spin-echo; (2) the breath-hold, multislice SSFSE or HASTE technique; and (3) the respiratory-triggered, 3D-FSE technique. Thick-slab, single-slice, T2-weighted MRCP images were obtained in the coronal, coronal oblique, and sagittal planes in at least six planes. Thin-slab, multislice, T2-weighted MRCP images were obtained in the coronal plane. Fifteen sections were acquired per breath-hold (volumes of coverage, 60 mm). The image data were then transferred to a workstation (Advanced Workstation, GE Medical or Leonardo, Siemens), and the 3D MRCP images were reconstructed using a maximum intensity projection algorithm to produce oblique images.

Dynamic images were obtained using a fat-suppressed, 3D GRE sequence, i.e., liver acquisition with volume acceleration, LAVA, GE Medical Systems or volume interpolation with breath-hold examination, VIBE, Siemens Medical Solutions, before and after administration of 0.1 mmol of gadobenate dimeglumine (MultiHance, Gd-BOPTA; Bracco SpA, Milan, Italy) per kilogram of the patient's body weight and with an injection rate of 2 mL/s. For timing of the contrast injection, an MR fluoroscopy technique was used which allows real-time visualization of the heart and aorta during repetitive measurements at the same coronal position and with using a T1W GRE sequence. The arterial

Table 2. MR parameters

MR scanner	T2WI	T1 W GRE	SS MRCP	MS MRCP	3D MRCP	FS-3D T1 W GRE	DWI[a]
Signa Excite HDX ($n = 27$)							
TR (ms)	∞	145	2800	∞	4000	5.2	3100
TE (ms)	110	2.0/4.2(OP/IP)	110	110	693	2.5	55
ETL	240	1	240	240	105	1	1
FA	150°	70°	150°	150°	180°	12°	90°
Slab thickness	7	7	50	2	1.0–1.4	2.5	7
FOV (mm)	300–350	300–350	220	200–240	256–320	300–350	380
Matrix	256×192	320×224	256×256	256×320	320×320	320×192	160×160
Verio ($n = 12$)							
TR (ms)	900	4.0	2500	2500	2000	3.2	3100
TE (ms)	149	1.3/2.2(OP/IP)	110	909	815	1.2	55
ETL	256	1	256	256	69	1	1
FA	130°	9°	130°	130°	130°	11°	90°
Slab thickness	7	3	50	0.9	0.9	3	7
FOV (mm)	300–380	300–380	220	200	380	300–380	380
Matrix	384×307	320×288	384×307	384×307	384×366	384×307	160×160

[a] b values of 0 and 500 s/mm^2

phase images were obtained 8 s after the arrival of the gadolinium-bolus was detected in the aorta. Arterial, portal venous, and delay-phase images were obtained serially at 20–40 s, 45–65 s, and 3–5 min, respectively, after contrast injection.

Among these 39 patients, 30 underwent DWI. DWI was performed on either a 1.5 T (Signa Excite HDX, GE Medical Systems, Milwaukee, WI, USA, $n = 18$) or on a 3 T (Verio, Siemens Medical Solutions, Erlangen, Germany, $n = 12$) superconducting system. The images were obtained using multisection, single-shot, spin-echo, echo-planar imaging with a spectral presaturation-attenuated, inversion-recovery, fat-suppressed pulse sequence during free-breathing scanning using a body coil with b values of 0 and 500 s/mm^2. All separate image series were acquired with diffusion weighting in the axial direction using three-directional diffusion gradients. The apparent diffusion coefficient (ADC) values ($\times 10^{-3}$ mm^2/s) were calculated as follows: ADC $= (1/(b_1 - b_0))$ ln(S_0/S_1).

Image analysis

MRI was retrospectively analyzed by two, board-certified radiologists (JHK, HWE). These two radiologists have served primarily as attending, abdominal radiologists and each has 11 years of clinical experience with abdominal MRI as part of their daily clinical and research practice. All images were reviewed on a Picture Archiving and Communications System (PACS) workstation monitor (m-view, Marotech, Seoul, Korea). The two radiologists retrospectively and independently reviewed each patient's MRI images. Both reviewers knew that the patients had undergone surgery for PNET, although they were blinded to all of the patients' detailed surgical and pathology findings.

The two radiologists retrospectively and independently accessed the T-stage and the lymph node metastasis. The largest diameter of each tumor and the location of the pancreatic lesions were also recorded. The reviewers also assessed the MRI findings, including the tumor margin (well-circumscribed vs. ill-defined borders), SI on the T2WI, tumor enhancement patterns (homogeneous vs. heterogeneous), the presence of cystic change, the presence of diffusion restriction on the DWI, contrast enhancement seen on the arterial phases, venous phases, and delayed phases compared with the adjacent pancreatic parenchyma. The presence of dilated pancreatic duct and bile duct were also recorded.

We used the T-staging for pancreatic PNET according to the AJCC (American Joint Committee on Cancer) 7th edition [14]. The T-stage of pancreatic cancer is defined by the tumor size and its local spread. Stage T1 tumors are confined to the pancreas and <2 cm in the largest diameter. In stage T2, the tumor diameter exceeds 2 cm in diameter, although it is still confined to the pancreatic gland. In stage T3, there is local tumor invasion into the peripancreatic fatty tissue and/or tumor infiltration into the duodenum or the common bile duct, but without involvement of the celiac axis or the superior mesenteric artery. In stage T4, the tumor involves the celiac axis or the superior mesenteric artery and this is the unresectable status. Lymph nodes are considered positive when there is a short-axis diameter greater than 5 mm or when there is necrosis, regardless of its size.

The ADC value of pancreatic masse was also objectively measured by another reviewer (YJK) who did not participate in the qualitative image analysis. To obtain the ADC values, regions of interest (ROIs) were placed on the ADC maps and were as large as possible within the three portions of the lesion (mean circular ROI, 74.8 + 52 mm^2), after which the average ROI values were obtained.

Table 3. Pathologic results of the PNET

	No. ($n = 39$)
Mean tumor size (cm)*	3.8 ± 2.1 cm
Tumor grade according to WHO classification	
PNETG1	24 (62%)
PNETG2	12 (31%)
PNEC	3 (8%)
T-stage	
T-1	9 (23%)
T-2	16 (41%)
T-3	14 (36%)
N-stage	
N0	36 (92%)
N1	3 (8%)

* Mean tumor size ± standard deviation

Statistical analysis

The relationship of the MR findings, tumor grade according to the WHO 2010 classification, and the T-, N-stage were assessed using Chi square tests and the Kruskal–Wallis test. Statistical significance was assumed at a confidence level of 0.05. The accuracy of the T-staging and the presence of lymph node metastasis were assessed using the McNemar test. To assess interobserver agreement, we performed a simple κ analysis of each of the imaging techniques. The degree of interobserver agreement, as indicated by the κ values, was interpreted as follows: 0–0.20, slight agreement; 0.21–0.40, fair agreement; 0.41–0.60, moderate agreement; 0.61–0.80, substantial agreement; and 0.81–1, almost perfect agreement. Differences in the accuracy of determining the tumor size as seen on MRI and that of the surgical specimen, were assessed using the paired T test. The diagnostic performance of the ADC for differentiating the tumor grade was evaluated using the receiver operating characteristic (ROC) curve (Az). Statistically significant MR findings associated with PNEC ($P < 0.5$) were further analyzed using multivariate logistic regression analysis. ROC curve analysis and the McNemar test were performed using MedCalc statistical software (version 6.15, MedCalc) for Windows (Microsoft), and other statistical analyses were conducted using an SPSS software package (version 14.0, SPSS).

Table 5. Diagnostic accuracy of MRI for T-stage and N-metastasis

	Correct staging	Overstaging	Understaging	Interobserver agreement
T-stage				0.78
R-1	30 (77%)	2 (5%)	7 (18%)	
R-2	33 (85%)	1 (3%)	5 (13%)	
N-metastasis				0.79
R-1	36 (92%)	2 (5%)	1 (3%)	
R-2	34 (87%)	4 (10%)	1 (3%)	

R Reader

Results

The tumor grade according to the WHO classification consisted of PNET grade 1 in 24 patients (62%), PNET grade 2 in 12 patients (31%), and PNEC in three patients (8%). The T-stage of the PNET consisted of T1 in nine patients (23%), T2 in 16 (41%), and T3 in 14 (36%). Node metastasis was confirmed in three patients (8%). Table 3 summarizes the pathology results of the PNET we identified. Table 4 summarizes the relationship between the WHO tumor classification and the T-stage, node metastasis, and tumor size. The T-stage closely correlated to the tumor grade ($P < 0.001$). All PNECs were of the T-3 stage, and eight patients with PNET grade 2 (67%) showed the T-3 stage, whereas only three patients with PNET grade 1 (13%) showed the T-3 stage. Node metastasis showed no statistical difference according to the tumor grade ($P < 0.565$). Regarding tumor size, PNEC (9.46 ± 9.5 cm) was larger than that of PNET grade 1 (2.98 ± 1.4 cm) or grade 2 (4.34 ± 3.4 cm) without statistical significance ($P = 0.252$).

Table 5 summarizes the diagnostic accuracy of MRI for assessing the T-stage and the presence of lymph node metastasis. The accuracy for determining the T-stage was 77% ($n = 30$) for reader 1 and 85% ($n = 33$) for reader 2 with moderate interobserver agreement ($\kappa = 0.78$). The overstage rate was 5% ($n = 2$) for reader 1 and 3% ($n = 1$) for reader 2. The understage rate was 18% ($n = 7$) for reader 1 and 13% ($n = 5$) for reader 2. The understaging of T3 as T2 on MR was most common for both readers 1 ($n = 6$) and 2 ($n = 4$) (Fig. 1). The accuracy for determining lymph node metastasis was

Table 4. Relationship between WHO tumor classification and T, N-stage, and tumor size

	PNETG1 ($n = 24$)	PNETG2 ($n = 12$)	PNEC ($n = 3$)	P
T-stage				
T-1 ($n = 9$)	8	1	0	$P < 0.001$*
T-2 ($n = 16$)	13	3	0	
T-3 ($n = 14$)	3	8	3	
N-metastasis				
N-0 ($n = 36$)	23	10	3	$P = 0.565$*
N-1 ($n = 3$)	1	2	0	
Tumor size (mm)	29.8 ± 14.6	43.4 ± 34.7	94.6 ± 95.1	$P = 0.252$**

* Linear-by-linear association
** Kruskal–Wallis Test
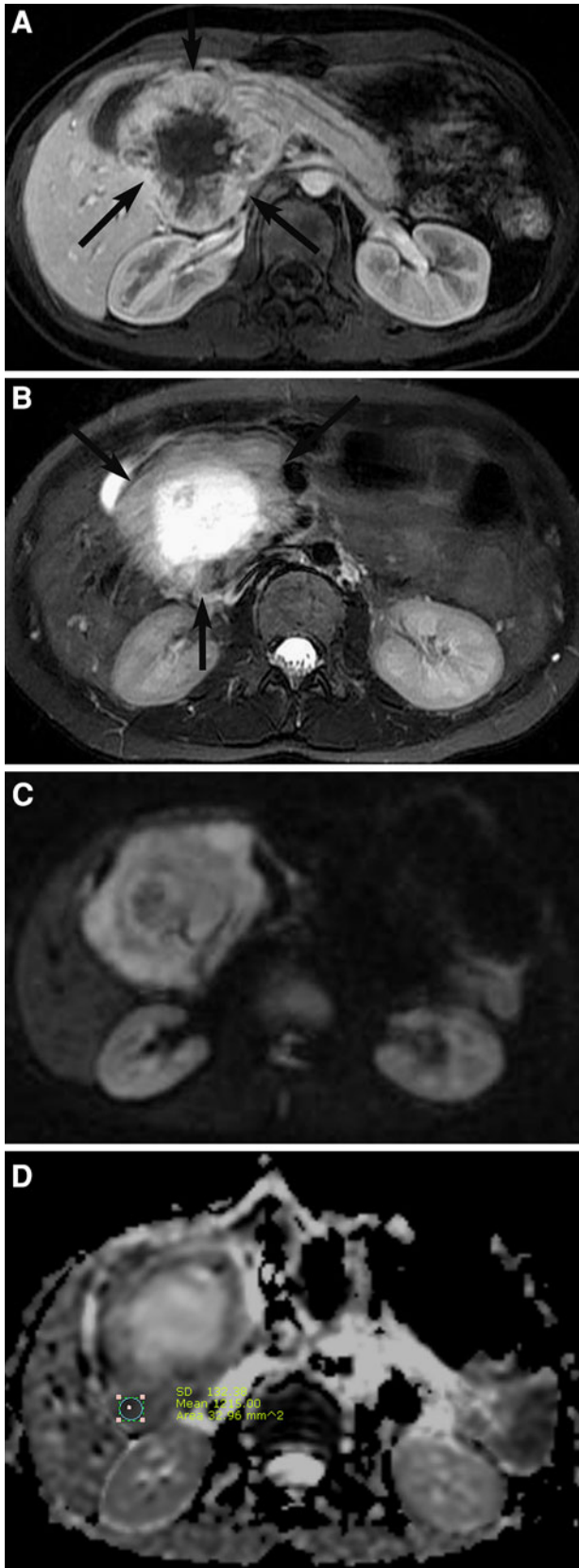
◄Fig. 1. A 57-year-old woman with PNET grade 2. Size of tumor was 11 cm at pathologic analysis. Tumor confirmed T3 stage with invasion into the peripancreatic fatty tissue. **A** Dynamic images using a fat-suppressed, 3D GRE sequence. On the arterial phase, a well-circumscribed mass located in the head of the pancreas shows arterial enhancement (*arrows*). Both radiologists interpreted this as T2 stage. **B** The mass shows high signal intensity with cystic degeneration on the fast spin-echo T2-weighted MR image (*arrows*). **C** Diffusion-weighted image (*b*—500 s/mm^2) shows the mass with high signal intensity and **D** an ADC value of 1.21×10^{-3} mm^2/s.

($n = 4$) for reader 2. The understage rate was 3% ($n = 1$) both readers 1 and 2. The mean diameter ($+ \text{SD}$) of the PNET was 3.9 ± 2.7 cm on MRI and 3.8 ± 2.1 cm on the surgical specimen. The tumor size determined by MR was not statistically different from the size determined by pathology studies ($P = 0.452$).

Table 6 summarizes the MRI findings of PNET. Statistically common MR findings for PNEC or PNET grade 2 compared with PNET grade 1, were found to be ill-defined borders ($P = 0.001$) and hypo-SI on the venous phase ($P = 0.016$) and delayed phase ($P = 0.019$). Two patients with PNEC (2/3, 67%) and two patients with PNET grade 2 (2/12, 17%) showed tumors with ill-defined borders, whereas all patients with PNET grade 1 showed tumors with well-circumscribed borders (Fig. 2). Two patients with PNEC (2/3, 67%) and four patients with PNET grade 2 (4/12, 33%) showed hypo-SI on the venous and delayed phases, whereas only two patients with PNET grade 1 (8%) showed hypo-SI on the venous and delayed phases. However, there were no independent MRI findings to predict PNEC or PNET grade 2 on the multivariate logistic regression analysis ($P < 0.5$). The bile duct or pancreatic duct dilatations are rare in PNET, in our study only 13% (5/39) of the patients showed bile duct dilatation and 21% (8/39) showed pancreatic duct dilatation.

DWI was performed on 20 patients with PNET grade 1 and on 10 patients with PNET grade 2. Fourteen patients with PNET grade 1 (70%) and nine patients with PNET grade 2 (90%) showed presence of diffusion restriction (Fig. 3). The ADC value showed a statistical difference between PNET grade 1 and grade 2 ($1.60 + 0.41 \times 10^{-3}$ mm^2/s vs. $1.24 + 0.127 \times 10^{-3}$ mm^2/s, $P = 0.007$) (Fig. 4). The area under the ROC curve (Az) for the ADC value for differentiating PNET grade 1 from grade 2, was 0.743, and using the cut-off ADC value of 1.22×10^{-3} mm^2/s, the sensitivity was 70% and the specificity was 86%.

Discussion

It is important to know the tumor stage and grade using preoperative MR imaging. It is widely accepted that surgical resection provides a high chance for long-term

92% ($n = 36$) for reader 1 and 87% ($n = 34$) for reader 2 with moderate interobserver agreement ($\kappa = 0.79$). The overstage rate was 5% ($n = 2$) for reader 1 and 10%

Table 6. MR findings of PPNET according to WHO tumor classification

MR findings	Tumor grade				P
	PNETG1 ($n = 24$)	PNETG2 ($n = 12$)	PNEC ($n = 3$)	Total	
Margin					
Well-circumscribed	24	10	1	35	0.001*
Ill-defined borders	0	2	2	4	
SI on T2WI					
Low	0	2	1	3	0.155*
Iso	4	1	0	5	
High	20	9	2	31	
Enhancement					
Homogeneous	6	3	1	10	0.951*
Heterogeneous	18	9	2	29	
Cystic degeneration	18	9	2	29	0.951
Enhance patterns					
Arterial					
Low	3	5	2	10	0.152*
Iso	7	2	0	9	
High	14	5	1	20	
Venous					
Low	2	4	2	8	0.016*
Iso	11	4	1	16	
High	11	4	0	15	
Delay					
Low	2	4	2	8	0.019*
Iso	10	4	1	15	
High	12	4	0	16	
CBD-dilatation	1	3	1	5	0.115
P-duct dilation	3	5	0	8	0.82

* Linear-by-linear association

survival for patients with PNETs [6, 15]. And as the T-stage of pancreatic cancer is defined by both the tumor size and the local spread, accurate T-staging is essential in order to differentiate resectable from unresectable PNET. According to previous reports, radiologic imaging is highly sensitive for assessing the T-stage in pancreatic adenocarcinoma [16]. However, to our knowledge no prior study has attempted to assess the MR accuracy of the T-, N-stage of PNET. As seen by our results, MRI is very useful for preoperatively evaluating the T-stage, node metastasis, and tumor size. In our study, the accuracy for determining the T-stage was 77% ($n = 30$) for reader 1 and 85% ($n = 33$) for reader 2. The T-stage of pancreatic cancer is defined by both the tumor size and its local spread. According to our study, MR has a tendency to understage tumors. The understaging of T3 as T2 on MR was most common for both readers 1 ($n = 6$) and 2 ($n = 4$). T3 was defined as local tumor invasion into the peripancreatic fatty tissue and/or tumor infiltration into either the duodenum or the common bile duct. In our patient, although there was tumor invasion into the peripancreatic fatty tissue, the duodenum or the common bile duct, most patients showed a well-defined tumor margin without increased signal intensity of the peripancreatic fat seen on MRI. These findings explain the misdiagnosis of T3 as T2. In our study, the accuracy for the N-stage was 92% ($n = 36$) and 87% ($n = 34$) and with moderate agreement ($\kappa = 0.79$). The tumor size (3.9 ± 2.7 cm) seen on MR was not statistically different

from the size determined by pathology (3.8 ± 2.1 cm, $P = 0.452$).

PNETs are heterogeneous in their morphological and biological features. Despite great behavioral differences between PNETs, they are grouped together as PNETs because of similarities in cell structure. We recently use both the WHO classification and the TNM staging to evaluate PNETs, both of which have advantages and disadvantages [1, 3–6, 15]. The WHO grading system is based on proliferation with the following definitions of mitotic count and Ki67 index: PNET grade 1 (mitotic count <2 per 10 HPF and/or $<2\%$ Ki-67 index); PNET grade 2 (mitotic count 2–20 per 10 HPF and/or 3–20% Ki-67 index); and NEC (mitotic count >20 per 10 HPF and/or $>20\%$ Ki-67 index) [2]. Use of the WHO classification is an important step toward defining the diverse tumor biology of NETs as it can represent a tumor's inherent malignant potential. However, WHO classification does not represent the tumor extent. In contrast, TNM staging is widely used for most types of pancreatic cancers and is based on the tumor extent. According to our study, T-stage statistically closely correlates to the WHO tumor grade ($P < 0.001$). The tumor size of PNEC (9.46 ± 9.5 cm) was also larger than the PNET grade 1 (2.98 ± 1.4 cm) or grade 2 (4.34 ± 3.4 cm), although without statistical significance ($P = 0.252$). However, the occurrence of node metastasis showed no statistically significant difference according to the tumor grade ($P < 0.565$).
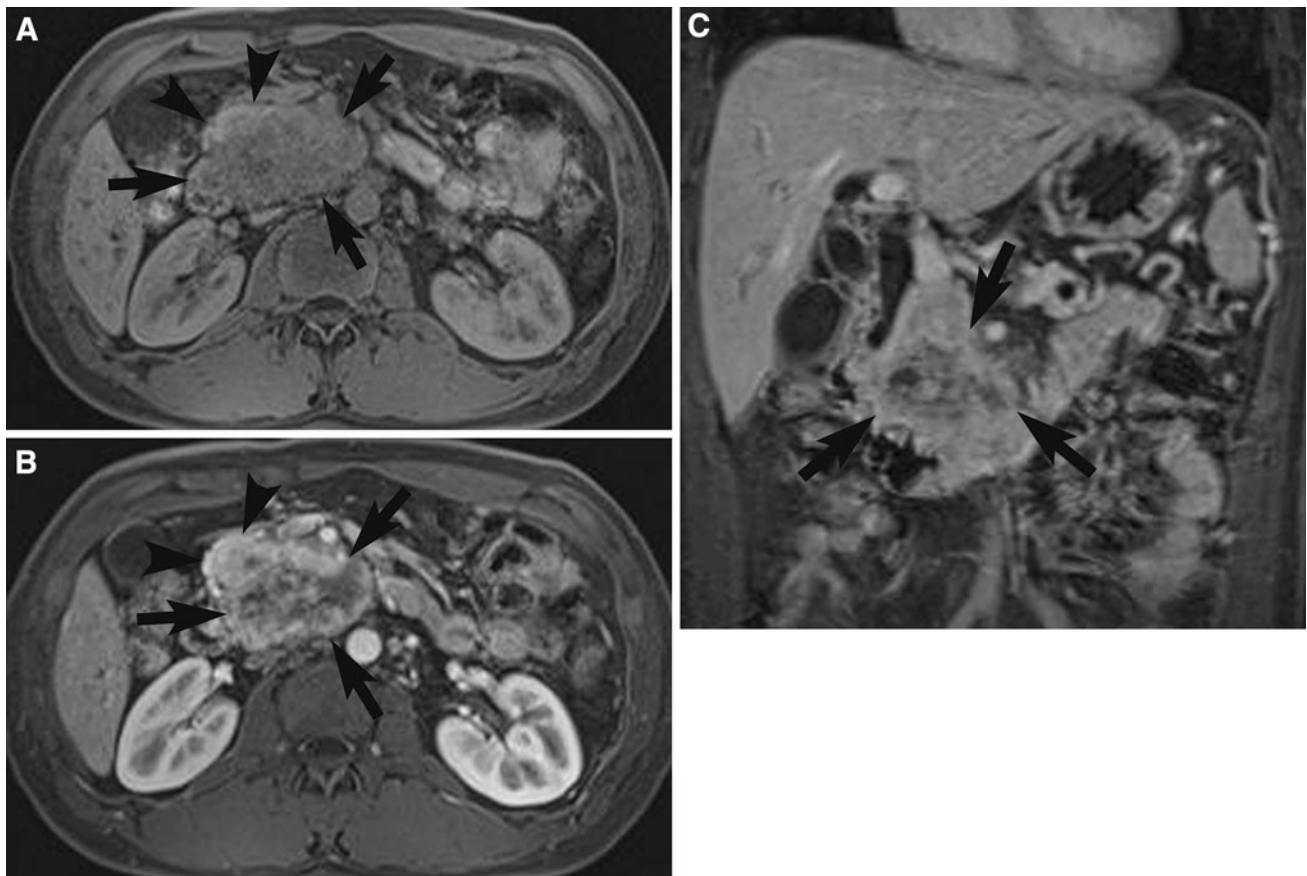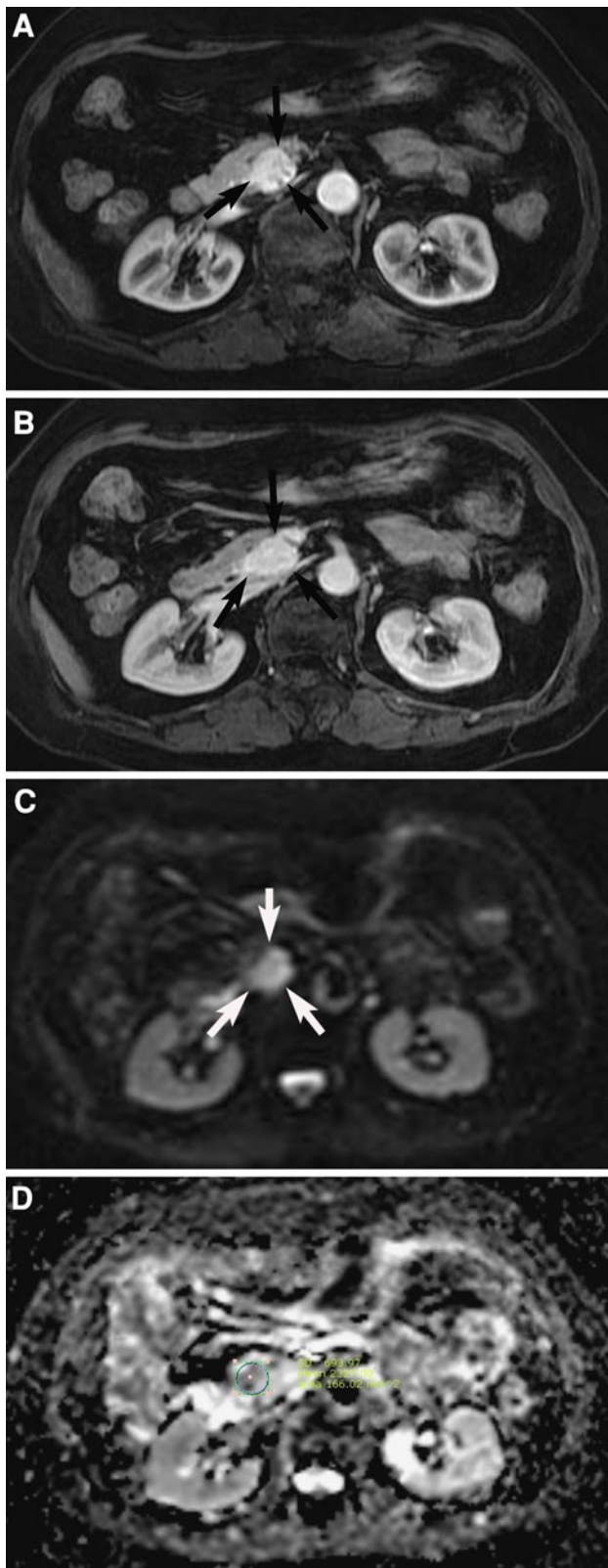
Fig. 2. A 65-year-old man with PNEC. Size of tumor was 9.2 cm at pathologic analysis. Tumor confirmed T3 stage with invasion into the common bile duct and the peripancreatic fatty tissue. **A–C** Dynamic images using a fat-suppressed, 3D GRE sequence. **A** On the precontrast phase, an ill-defined low signal intensity mass (*arrows*) compare with pancreatic parenchyma (*arrowheads*) is noted in the head of the pancreas. **B** On the arterial phase, the mass shows heterogenous low signal intensity (*arrows*) compared with pancreatic parenchyma (*arrowheads*). **C** The mass shows low signal intensity on the delayed phase (*arrows*) compared with pancreatic parenchyma. The dilated bile duct is noted. Both radiologists interpreted this as T3 stage.

According to previous reports, common MR findings of PNET include well-defined, low signal intensity on T1WI, high signal intensity on T2WI, and immediate intense enhancement on post-contrast images [8–11]. These results are similar to those described in our study, in which the common MR findings of PNET included a well-circumscribed margin (35/39), high signal intensity on T2WI (31/39), cystic degeneration with heterogeneous enhancement (29/38), arterial enhancement (20/39), and iso- to high-signal intensity on the portal and delayed phases (31/39). The previous reports also confirmed that biliary dilatation is uncommon in PNET, and which agrees with our study results which showed bile duct dilatation in 13% (5/39) and pancreatic duct dilatation in 21% (8/39).

It is important to predict the tumor grade using preoperative MR imaging as some of these tumors grow slowly and exhibit benign behavior, whereas others grow more rapidly and display malignant behavior. However,

PNECs are rare, accounting for less than 2%–3% of all PNETs. There are a few reports regarding PNEC [11, 17, 18]. Ichikawa et al. [17] reported that the PNECs seen in their study were large, i.e., with a mean diameter of 5.8 cm, and that they demonstrated minimal and homogeneous enhancement, thus mimicking pancreatic ductal adenocarcinoma, lymphoma, and metastatic disease. Although our study demonstrates a wide spectrum of morphological characteristics, signal characteristics, and enhancement patterns in PNET, our results show that statistically specific MR imaging findings for higher grade PNET included ill-defined borders ($P = 0.001$) and hypo-SI seen on the venous phase ($P = 0.016$) and the delayed phase ($P = 0.019$). Two patients with PNEC (2/3, 67%) and two patients with PNET grade 2 (2/12, 17%) showed tumors with ill-defined borders, whereas all patients with PNET grade 1 showed tumors with well-circumscribed borders. Two patients with PNEC (2/3, 67%) and four patients with PNET grade 2 (4/12, 33%)

◀ **Fig. 3.** A 47-year-old man with PNET grade 1. Size of tumor was 3.2 cm at pathologic analysis. Tumor confirmed T2 stage. **A**, **B** Dynamic images using a fat-suppressed, 3D GRE sequence. **A** On the arterial phase, a well-circumscribed mass located in the uncinate of the pancreas shows arterial enhancement (*arrows*). **B** The mass shows a well-defined tumor margin with high signal intensity on the venous phases (*arrows*). Both radiologists interpreted this as T2 stage. **C** Diffusion-weighted image (b—500 s/mm^2) shows the mass with high signal intensity (*arrows*) and **D** an ADC value of 2.3×10^{-3} mm^2/s.

The recent use of DWI in patients with abdominal disease provides promising results for tumor characterization [12, 13, 19, 20]. DWI detects the random motion of water molecules within biologic tissue and produces a representative ADC value, however, there are only a few published reports which assessed PNET using DWI. Wang et al. [13] recently reported that ADC correlates well with the Ki-67 labeling index and may thus help to predict the growth of endocrine tumors. They assessed 18 patients with PNETs. According to their results, PNEC had significantly lower ADC values than those of PNET ($1.00 + 0.19 \times 10^{-3}$ mm^2/s vs. $1.75 + 0.53 \times 10^{-3}$ mm^2/s, $P < 0.01$). They suggested that variation in the ADC values of endocrine tumors may be influenced by the combination of tumor cellularity, the proportion of cytoplasm, and extracellular fibrosis. In our study, the ADC value showed a statistically significant difference between PNET grade 1 and grade 2 ($1.60 + 0.41 \times 10^{-3}$ mm^2/s vs. $1.24 + 0.127 \times 10^{-3}$ mm^2/s, $P = 0.007$). The area under the ROC curve (Az) for the ADC value differentiating PNET grade 1 from grade 2, was 0.743, and using the cut-off ADC value as 1.22×10^{-3} mm^2/s, the sensitivity was 70% and the specificity was 86%. Despite its promising potential for predicting the tumor grade,
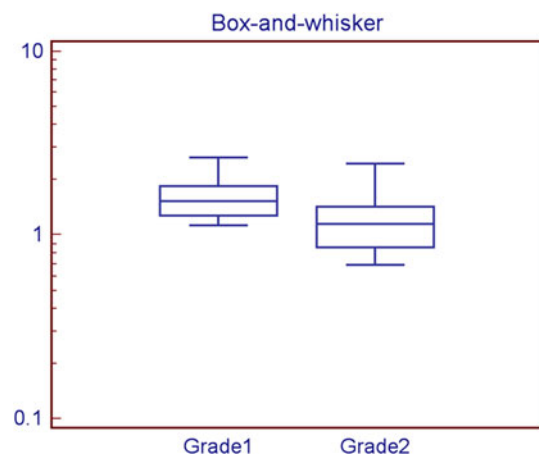

Fig. 4. Box–whisker plots of the ADC values in patients with PNET grade 1 and grade 2. The ADC value showed a statistical difference between PNET grade 1 and grade 2 ($1.60 + 0.41 \times 10^{-3}$ mm^2/s vs. $1.24 + 0.127 \times 10^{-3}$ mm^2/s, $P = 0.007$).

showed hypo-SI on the venous and delayed phases, whereas only two patients with PNET grade 1 (8%) showed hypo-SI on the venous and delayed phases.

further studies with a larger patient population will be needed in order to address the value of DWI in PNET.

Our study had a number of limitations. First, our study includes only surgically proven patients with PNET; those with PNET who did not undergo surgery were excluded. Therefore, our study population did not reflect the entire spectrum of PNET, e.g., our study included only three patients with PNEC. Although the incidence of PNEC is rare, many patients with PNEC are combined with metastasis and, therefore, do not undergo surgery. Second, our study was retrospective and undertaken at a single institution and which may have introduced unintended biases. One of them is that not all patients underwent DWI As only 20 patients with PNET grade 1 and 10 patients with PNET grade 2 underwent DWI. There were no study patients with PNEC who underwent DWI. Further studies with a larger sample size will be needed in order to address the value of DWI in PNET.

Despite these limitations, to our knowledge, there are no dedicated MRI studies preoperatively predicting the tumor grade and TN-stage of PNET. We believe that MR imaging can provide the comprehensive information needed for the preoperative imaging diagnosis of the tumor grade and stage in PNET, and which is clinically important for predicting the patient prognosis and determining the optimal surgical strategy. Our study demonstrates that ill-defined tumor borders and hypo-SI seen on the venous and delayed phases are common findings of higher grade PNET and that the ADC value is helpful for differentiating PNET grade 1 from grade 2. MR imaging is useful for the preoperative evaluation of the T-stage, N-stage, and tumor size of PNET, especially as the T-stage showed a statistically significant difference depending on the tumor grade.

Conflict of interest. No conflict of interest.

References

1. Ehehalt F, Saeger HD, Schmidt CM, Grützmann R (2009) Neuroendocrine tumors of the pancreas. Oncologist 14(5):456–467
2. Bosman FT, Carneiro F, Hruban RH, Theise N (2010) *WHO classification of tumours of the digestive system.* Lyon: IARC Press
3. Liszka , Pająk J, Mrowiec S, et al. (2011) Discrepancies between two alternative staging systems (European Neuroendocrine Tumor Society 2006 and American Joint Committee on Cancer/Union for International Cancer Control 2010) of neuroendocrine neoplasms of the pancreas. A study of 50 cases. Pathology-Research and Practice 207(4):220–224
4. Rindi G, Klöppel G, Alhman H, et al. (2006) TNM staging of foregut (neuro) endocrine tumors: a consensus proposal including a grading system. Virchows Arch 449(4):395–401
5. Rindi G, Klöppel G, Couvelard A, et al. (2007) TNM staging of midgut and hindgut (neuro) endocrine tumors: a consensus proposal including a grading system. Virchows Arch 451(4):757–762
6. Sellner F, Thalhammer S, Stättner S, Karner J, Klimpfinger M (2011) TNM stage and grade in predicting the prognosis of operated, non-functioning neuroendocrine carcinoma of the pancreas—a single-institution experience. J Surg Oncol 104(1):17–21
7. Bushnell DL, Baum RP (2011) Standard imaging techniques for neuroendocrine tumors. Endocrinol Metab Clin North Am 40(1):153
8. Caramella C, Dromain C, De Baere T, et al. (2010) Endocrine pancreatic tumours: which are the most useful MRI sequences? Eur Radiol 20(11):2618–2627
9. Herwick S, Miller FH, Keppke AL (2006) MRI of islet cell tumors of the pancreas. AJR Am J Roentgenol 187(5):W472–W480
10. Ku YM, Shin SS, Lee CH, Semelka RC (2009) Magnetic resonance imaging of cystic and endocrine pancreatic neoplasms. Top Magn Reson Imaging 20(1):11–18
11. Lewis RB, Lattin GE, Paal E (2010) Pancreatic endocrine tumors: radiologic-clinicopathologic correlation. Radiographics 30(6):1445–1464
12. Lee SS, Byun JH, Park BJ, et al. (2008) Quantitative analysis of diffusion-weighted magnetic resonance imaging of the pancreas: usefulness in characterizing solid pancreatic masses. J Magn Reson Imaging 28(4):928–936
13. Wang Y, Chen ZE, Yaghmai V, et al. (2011) Diffusion-weighted MR imaging in pancreatic endocrine tumors correlated with histopathologic characteristics. J Magn Reson Imaging 33(5):1071–1079
14. Edge SB, Byrd DR, Compton CC, et al. (2010) *AJCC cancer staging manual*, 7th edn. New York: Springer, pp 285–296
15. Ekeblad S, Skogseid B, Dunder K, Öberg K, Eriksson B (2008) Prognostic factors and survival in 324 patients with pancreatic endocrine tumor treated at a single institution. Clin Cancer Res 14(23):7798–7803
16. Park HS, Lee JM, Choi HK, et al. (2009) Preoperative evaluation of pancreatic cancer: comparison of gadolinium-enhanced dynamic MRI with MR cholangiopancreatography versus MDCT. J Magn Reson Imaging 30(3):586–595
17. Ichikawa T, Federle M, Ohba S, et al. (2000) Atypical exocrine and endocrine pancreatic tumors (anaplastic, small cell, and giant cell types): CT and pathologic features in 14 patients. Abdom Imaging 25(4):409–419
18. Rha SE, Jung SE, Lee KH, et al. (2007) CT and MR imaging findings of endocrine tumor of the pancreas according to WHO classification. Eur J Radiol 62(3):371–377
19. Balci NC, Perman WH, Saglam S, et al. (2009) Diffusion-weighted magnetic resonance imaging of the pancreas. Top Magn Reson Imaging 20(1):43
20. Mottola JC, Sahni VA, Erturk SM, et al. (2012) Diffusion-weighted MRI of focal cystic pancreatic lesions at 3.0-Tesla: preliminary results. Abdom Imaging 37(1):110–117